

Simulation and optimization for a 30-MeV electron accelerator driven neutron source

LIN Zuokang^{1,2} SUN Guomin^{1,2} CHEN Jingen¹ LIU Guimin¹ DAI Zhimin^{1,*}

¹Shanghai Institute of Applied Physics, Chinese Academy of Sciences, Jiading Campus, Shanghai 201800, China

²University of Chinese Academy of Sciences, Beijing 100049, China

Abstract A neutron source driven by electron accelerator is proposed in Shanghai Institute of Applied Physics (SINAP). The facility is planned for the study of nuclear data in Thorium-Uranium cycling system, and for material research. A detailed simulation of the neutron source is performed for the program to get the neutron generation maximum economically. Several parameters of the facility, which affect the neutron yield and the neutron escape from outer surface of the target, are analyzed respectively. Besides, the yielding neutron spectrum and the escaping neutron angular distribution are calculated and discussed.

Key words Neutron source, Neutron yield, Neutron escape, Neutron spectrum

1 Introduction

A neutron source driven by a 30 MeV electron accelerator is proposed in Shanghai Institute of Applied Physics. The neutron source, expected with a strength of $10^{13}\sim 10^{14}$ n/s (4π), can be used in the study of nuclear data^[1] for Thorium-Uranium cycling system, and in material research. An electron accelerator is cheap and compact comparatively. Furthermore, it can bring advantages in terms of reliability^[2]. When the incident particle has the energy of 1000 MeV, the neutron yield is 20 neutrons/proton and 0.4 neutrons/electron. While the incident particle energy is 20 MeV, the neutron yield is 0.004 neutrons/proton and 0.002 neutrons/electron. It is obvious that the difference of neutron yield between proton and electron decreases as the incident particle energy decreases. The neutron yield from an electron accelerator driven neutron source is close to a proton accelerator driven source, when the incident particle energy is as low as about 20 MeV. As calculated, 20 MeV electron beam at a power of 20 kW with the tungsten target can produce neutrons with strength of

10^{13} n/s (4π). So, it is advisable to choose an electron accelerator driver while the intensity of neutron source is met.

Since the aim is to maximize the generation of neutron economically in this work, a detailed physical analysis of the target is performed. Incident particle energy, beam size, target material, geometry, and coolant influence, which affect the neutron yield and the neutron escape from outer surface of the target, will be optimized. This work will focus on simulating target-models in different conditions for the target optimization. In the end, the flux and escaping angular of the neutron source are presented.

2 Simulation model

The main interactions which have influence with the neutron generation can be described by two steps^[3]. Firstly, electrons are slowed down and stopped in the target material; simultaneously gamma is produced by bremsstrahlung. Secondly, neutrons are produced by photonuclear (γ, n) and photon-fission (γ, f) reactions. And then, a part of neutrons penetrate the target material and escape from the target.

* Corresponding author. E-mail address: daizhimin@sinap.ac.cn

Received date: 2011-12-05

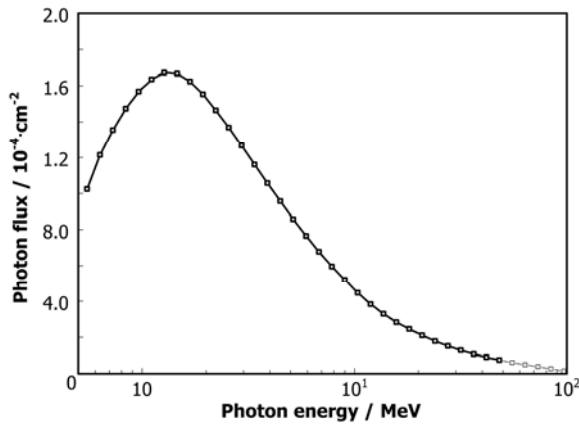


Fig.1 Gamma spectrum in thorium target bombarded by 100-MeV electron.

A photon spectrum produced in thick thorium target with 100 MeV incident electrons, simulated by Monte Carlo N-Particle transport code, is displayed in Fig.1. The spectrum with photon energy under 0.5 MeV is ignored in simulation, due to the neutron yield threshold. The peak of photon spectrum produced by Bremstrahlung is about 1.5 MeV as shown in Fig.1, while the photonuclear (γ, n) reaction cross section has a peak around 12 MeV for heavy nuclei and its curve has a Gaussian form distribution from about 5 MeV to 35 MeV^[3]. Since a part of Bremstrahlung-photons come across the threshold of (γ, n) reaction in the target, there are neutrons produced. Besides (γ, n) reaction, Photon-fission (γ, f) reaction also produces neutrons, for which there is a threshold of about 6 MeV in most of fertile or fissile nuclei.

The simplest model simulated by Monte Carlo N-Particle transport code is built for benchmarking, as shown in Fig.2. It is a cylinder target having 50 cm length and 12 cm diameter. And the 100 MeV incident electron beam diameter is 10 cm. Besides, photons of energy below 0.5 MeV, which have no contribution in

neutron generation, are cut off in simulation to improve the code running efficiency.

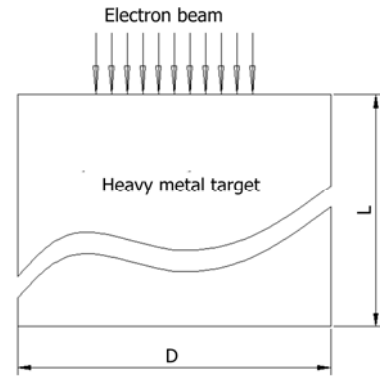


Fig.2 Benchmark target model.

The data from an IAEA technical report^[4] are used in Table 1. The comparisons of the neutron yield in 4 selected target materials are presented. The results, simulated by Monte Carlo N-Particle transport code, are in good agreement with the results of experimental data, as shown in Table 1. The different target materials do not deflect the shape of the spectra much, as shown in Fig.3.

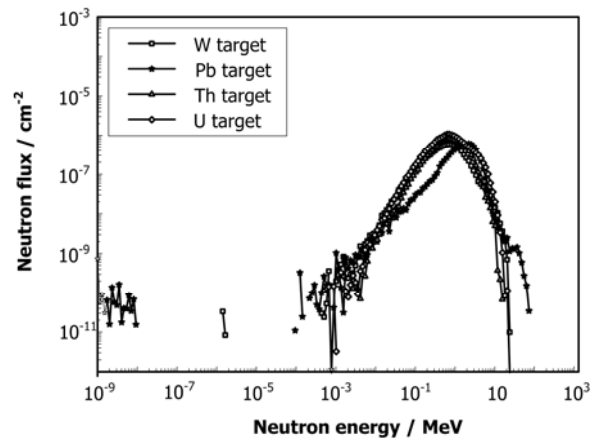


Fig.3 Neutron yield spectra on different material targets with 100 MeV incident electron.

Table 1 Comparisons of neutron yield between simulation and experiment with 100-MeV electron beam

Thick target materials	Tungsten (W)	Lead (Pb)	Thorium (Th)	Uranium (U)
Results from Stanford Linear Accelerator Center by W.P. Swanson(n/e) [4]	$2.72 \cdot 10^{-2}$	$2.56 \cdot 10^{-2}$ $\sim 5.12 \cdot 10^{-2}$	$4.64 \cdot 10^{-2}$	$6.24 \cdot 10^{-2}$
Results of Neutron yield simulated in this work(n/e)	$3.18 \cdot 10^{-2}$	$3.09 \cdot 10^{-2}$	$4.68 \cdot 10^{-2}$	$6.47 \cdot 10^{-2}$

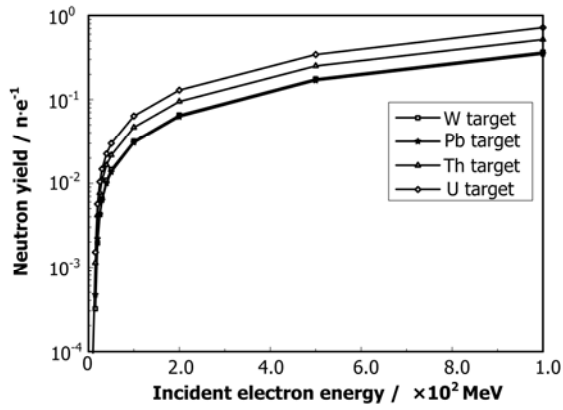


Fig.4 Neutron yields of different materials target with incident energy ranging from 10 MeV to 1 GeV.

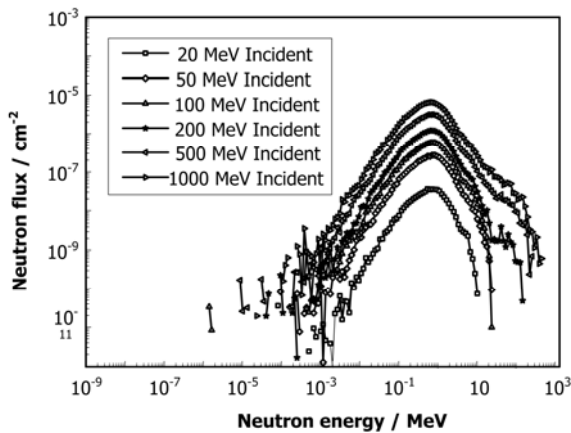


Fig.5 Neutron yield spectra on W target with different incident energy electrons.

From the photonuclear (γ, n) cross section curve and the threshold of the Photon-fission reaction (γ, f), the incident electrons between 10 MeV to 1 GeV are simulated in the target model for comparison of neutron yields. In Fig.4, the neutron yields of natural uranium, thorium, lead and tungsten targets with incident energy ranging from 10 MeV to 1 GeV are

presented. The neutron yield grows sharply when the incident electron energy increases from 10 MeV to 50 MeV, and almost grows linearly as the incident energy beyond 100 MeV. In addition, the neutron yields in natural uranium and thorium targets are higher than those in tungsten and lead targets, because uranium and thorium are fertile or fissile materials in which the photon-fission (γ, f) reactions contribute to the neutron yield.

As the energy of incident electron grows, the upper limit energy of the yield neutron grows too, seen in Fig.5. However, incident electrons with different energies almost produce neutrons in similar shape spectrum curves, with the same peak at about 1 MeV.

3 Optimization of beam size and target geometry

Based on the above simulation, the optimization of beam size and target geometry is performed for the tungsten target bombarding with a 30 MeV incident electron beam. Though in the thorium and uranium targets more neutrons can be produced, thorium and uranium will not be considered in this work because there is extra radioactive substance produced in these targets in the experiment processes.

In the beam size optimization, the cylinder model geometry size is kept at 5 cm diameter and 5 cm length. With 30 MeV electron beam bombarding tungsten target used in the model, the simulated neutron yield and escape with different beam sizes are presented in Table 2.

Table 2 Neutron yield and escape with different incident electron beam sizes

(Electron energy 30 MeV, Tungsten (W) target, D=5.0 cm, L=5.0 cm)						
Electron beam diameter(cm)	1.0	1.5	2.0	2.5	3.0	4.6
Total neutron yield(n/e)	$7.1716 \cdot 10^{-3}$	$7.1847 \cdot 10^{-3}$	$7.1837 \cdot 10^{-3}$	$7.1817 \cdot 10^{-3}$	$7.1676 \cdot 10^{-3}$	$6.8058 \cdot 10^{-3}$
Escape(n/e)	$7.0682 \cdot 10^{-3}$	$7.0813 \cdot 10^{-3}$	$7.0828 \cdot 10^{-3}$	$7.0813 \cdot 10^{-3}$	$7.0711 \cdot 10^{-3}$	$6.7253 \cdot 10^{-3}$

As shown in Table 2, there is the best neutron escaping from the target outer surface at beam size 2cm diameter, while 30 MeV incident electron bombards into a cylinder tungsten target, $D=5$ cm, $L=5$ cm. In fact, when 30 MeV incident electron beam bombards a cylinder tungsten target, $D=10$ cm and

$L=10$ cm, an electron beam size of about 2 cm can also reach the best neutron escaping. So in the target geometry optimization, the beam size is fixed at 2 cm.

In target geometry optimization, the neutron generation should be considered simultaneously in the radial and in the axial directions. Firstly, with the fixed

length of 5 cm, variable diameter targets have different neutron yielding and escaping. The neutron escape reaches the maximum, when the diameter is 6 cm. Secondly, with the fixed diameter of 6 cm. And variable length targets have different escape values. As shown in Table 3, the neutron escape is max when the length is 7.5 cm. Therefore, an optimized neutron escape will be obtained in a target with 6 cm diameter and 7.5 cm length.

Considering taking away the energy deposition in the target, a coolant system has to be designed. The target configuration is studied, and a circular-disks

target is chosen, seen in Fig.6. The coolant with room temperature water splits among narrow gaps between target disks to cool them. Various target plate and coolant channel thicknesses are evaluated and an optimal neutron yield is obtained with nominally 1.5 mm narrow coolant channels between 10 target disks, which thickness are 3 mm, 3 mm, 3 mm, 3 mm, 4 mm, 5 cm, 6 mm, 9 mm, 14 mm, 25mm. With the coolant system, the neutron is slightly moderated as the Fig.7 shows, and the neutron escaping from the target outer-surface is about 2% discount.

Table 3 Neutron yield and escape in variable diameters and lengths

Fixed length of 5.0 cm			Fixed diameter of 6.0 cm		
Diameter / cm	Total neutron yield (n/e)	Escape (n/e)	Length / cm	Total neutron yield (n/e)	Escape (n/e)
2.0	$5.644 \cdot 10^{-3}$	$5.615 \cdot 10^{-3}$	1.0	$4.717 \cdot 10^{-3}$	$4.687 \cdot 10^{-3}$
2.5	$6.405 \cdot 10^{-3}$	$6.362 \cdot 10^{-3}$	2.0	$6.475 \cdot 10^{-3}$	$6.407 \cdot 10^{-3}$
3.0	$6.704 \cdot 10^{-3}$	$6.649 \cdot 10^{-3}$	2.5	$6.748 \cdot 10^{-3}$	$6.668 \cdot 10^{-3}$
3.5	$6.932 \cdot 10^{-3}$	$6.864 \cdot 10^{-3}$	3.0	$6.951 \cdot 10^{-3}$	$6.859 \cdot 10^{-3}$
4.0	$7.068 \cdot 10^{-3}$	$6.989 \cdot 10^{-3}$	3.5	$7.087 \cdot 10^{-3}$	$6.985 \cdot 10^{-3}$
4.5	$7.122 \cdot 10^{-3}$	$7.034 \cdot 10^{-3}$	4.0	$7.161 \cdot 10^{-3}$	$7.052 \cdot 10^{-3}$
5.0	$7.184 \cdot 10^{-3}$	$7.083 \cdot 10^{-3}$	4.5	$7.221 \cdot 10^{-3}$	$7.107 \cdot 10^{-3}$
5.5	$7.216 \cdot 10^{-3}$	$7.107 \cdot 10^{-3}$	5.0	$7.234 \cdot 10^{-3}$	$7.116 \cdot 10^{-3}$
6.0	$7.234 \cdot 10^{-3}$	$7.116 \cdot 10^{-3}$	5.5	$7.255 \cdot 10^{-3}$	$7.133 \cdot 10^{-3}$
6.5	$7.218 \cdot 10^{-3}$	$7.092 \cdot 10^{-3}$	6.0	$7.254 \cdot 10^{-3}$	$7.130 \cdot 10^{-3}$
7.0	$7.225 \cdot 10^{-3}$	$7.091 \cdot 10^{-3}$	6.5	$7.263 \cdot 10^{-3}$	$7.138 \cdot 10^{-3}$
7.5	$7.253 \cdot 10^{-3}$	$7.109 \cdot 10^{-3}$	7.0	$7.266 \cdot 10^{-3}$	$7.139 \cdot 10^{-3}$
8.0	$7.242 \cdot 10^{-3}$	$7.090 \cdot 10^{-3}$	7.5	$7.271 \cdot 10^{-3}$	$7.142 \cdot 10^{-3}$
9.0	$7.232 \cdot 10^{-3}$	$7.063 \cdot 10^{-3}$	11.0	$7.272 \cdot 10^{-3}$	$7.140 \cdot 10^{-3}$
10.0	$7.253 \cdot 10^{-3}$	$7.069 \cdot 10^{-3}$	15.0	$7.272 \cdot 10^{-3}$	$7.139 \cdot 10^{-3}$

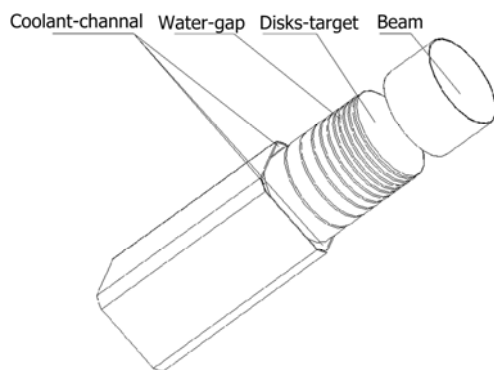


Fig.6 Schematic of disks-target model and coolant system.

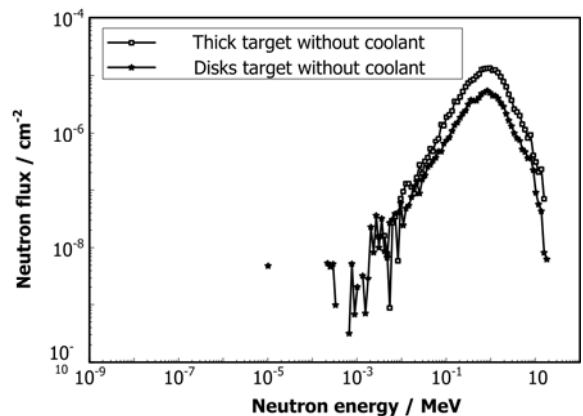


Fig.7 Neutron yield spectra on thick/disks target with 30 MeV incident electron.

4 Neutron flux distribution and escape angular distribution

After the optimizations, the simulation model of 30 MeV electron beam bombarding into tungsten target is performed. The neutron flux distributions in the target and the escaping angular distribution are extracted and the results are presented respectively in Figs.8, 9 and 11, in which all of the flux values are unitary by single incident electron.

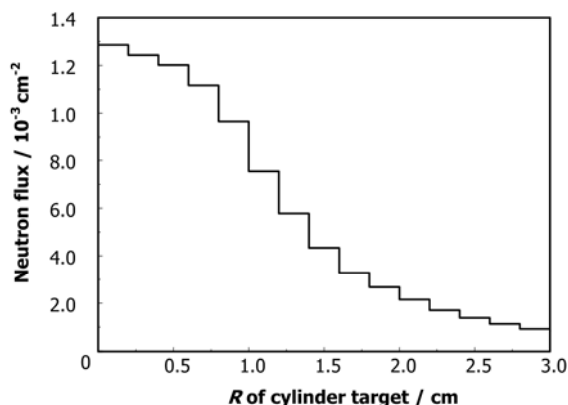


Fig.8 Neutron flux distribution in R direction.

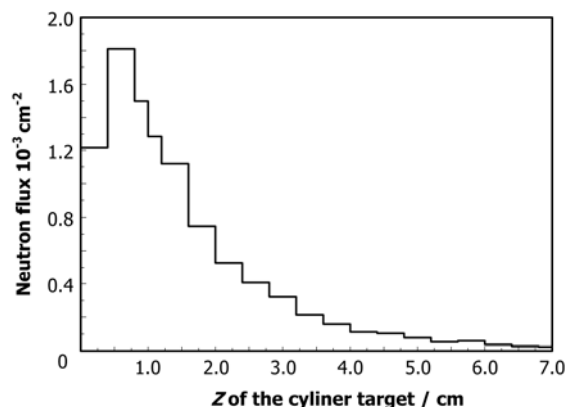


Fig.9 Neutron flux distribution in Z direction.

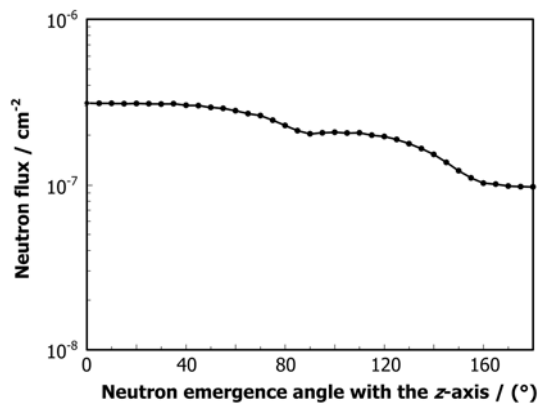


Fig.10 Escaping neutron angular distribution with Z axial.

The neutron detectors, set to ring detectors in the simulation models, are posited on r-z plane to form a circle ($R=50$ cm), and the neutron escaping angular distribution recorded by the detectors is shown in Fig.10. It indicates that neutron angular distribution from the electron beam driven neutron source is almost isotropic. In the optimized model, the neutron escape is $7.0 \cdot 10^{-2}$ n/e, i.e. with a 30-MeV incident electron beam at power of 30 kW producing neutrons with strength of $4.3 \cdot 10^{13}$ n/s (4π) in tungsten target.

5 Conclusion

In this work, a physical analysis of electron accelerator driven neutron source is presented. As the simulation results present, the neutron yield grows sharply when the incident electron energy increases from 10 MeV to 50 MeV, and almost grows linearly as the incident energy beyond 100 MeV. Different incident particle energy (10 MeV to 1 GeV) and target materials (heavy metals), which can vary neutron generation, hardly inflect the shape of the yielding neutron spectra. The incident electron beam size is fitted in 2 cm diameter and target geometry is optimized into 6 cm diameter and 7.5 cm length cylinder. After consideration of taking away the deposition energy, the target is altered into 10 disks with 1.5mm coolant gaps, filled with room temperature water, between each disk. The coolant slightly moderates the spectra of the yielding neutron, and makes the neutron escape 2% discount. The flux and emergence angular of the neutron source are presented to prove that the neutron source is almost isotropic.

Be summarized, a 30 MeV 30 kW incident electron beam is chosen to bombard into tungsten disks-target to produce neutrons in the facility, and it will supply a neutron source with strength of $4.3 \cdot 10^{13}$ n/s (4π) for experiment.

References

- 1 Kim G N, Kovalchuk V, Lee Y S, *et al.* Nucl Instr Meth Phys Res, 2002, **A485**: 458–467.
- 2 Yousry G, Igor B, Dmitry N. Nucl Instrum Meth Phys Res, 2006, **A562**: 870–874.
- 3 Jallu F. Nucl Instrum Meth Phys Res, 1999, **B155**: 373–381.
- 4 William P S. IAEA technical reports series, 1979, No.188.